Cell Reports

Report

Pak4 Is Required during Epithelial Polarity Remodeling through Regulating AJ Stability and Bazooka Retention at the ZA

Graphical Abstract

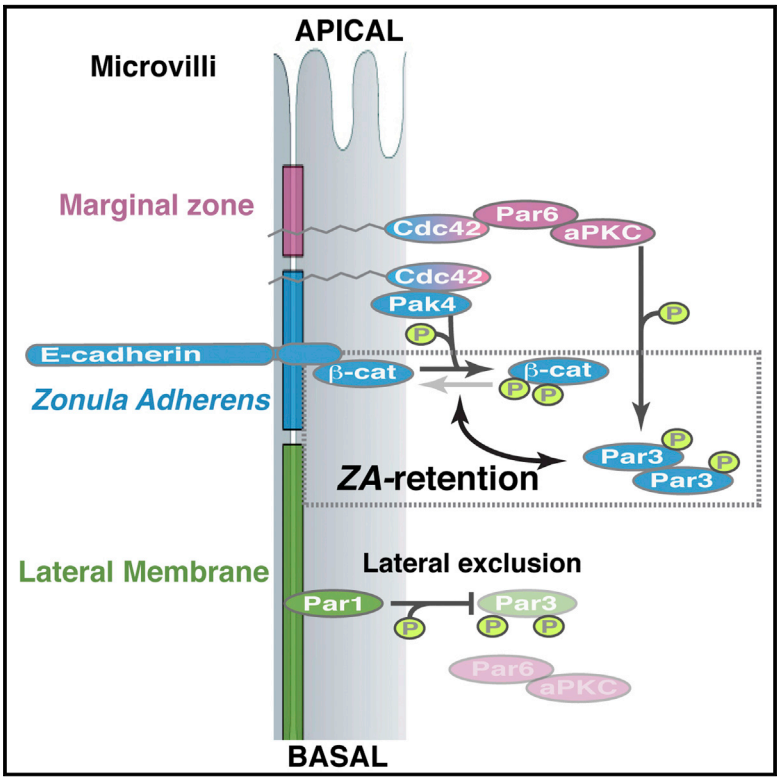

Highlights

- Pak4 regulates adherens junction accumulation at the zonula adherens
- Pak4 promotes Par3 (Bazooka) retention at the zonula adherens
- Par1 and Pak4 synergize in preventing lateral accumulation of Par3

Authors

Rhian F. Walther, Francisca Nunes de Almeida, Evi Vlassaks, Jemima J. Burden, Franck Pichaud

Correspondence

f.pichaud@ucl.ac.uk

In Brief

Walther et al. reveal a functional cross-talk pathway between the developing epithelial adherens junction and apical plasma membrane differentiation. The authors provide a molecular mechanism that explains how defects in cell-cell contact morphogenesis impact on epithelial polarity remodeling and maintenance.

Walther et al., 2016, Cell Reports *15*, 45–53
April 5, 2016
http://dx.doi.org/10.1016/j.celrep.2016.03.014

CellPress

Cell Reports
Report

Pak4 Is Required during Epithelial Polarity Remodeling through Regulating AJ Stability and Bazooka Retention at the ZA

Rhian F. Walther,[1] Francisca Nunes de Almeida,[1] Evi Vlassaks,[1] Jemima J. Burden,[1] and Franck Pichaud[1,*]
[1]MRC Laboratory for Molecular Cell Biology, University College London, Gower Street, WC1E 6BT London, UK
*Correspondence: f.pichaud@ucl.ac.uk
http://dx.doi.org/10.1016/j.celrep.2016.03.014

SUMMARY

The ability of epithelial cells to assemble into sheets relies on their zonula adherens (ZA), a circumferential belt of adherens junction (AJ) material, which can be remodeled during development to shape organs. Here, we show that during ZA remodeling in a model neuroepithelial cell, the Cdc42 effector P21-activated kinase 4 (Pak4/Mbt) regulates AJ morphogenesis and stability through β-catenin (β-cat/Arm) phosphorylation. We find that β-catenin phosphorylation by Mbt, and associated AJ morphogenesis, is needed for the retention of the apical determinant Par3/Bazooka at the remodeling ZA. Importantly, this retention mechanism functions together with Par1-dependent lateral exclusion of Par3/Bazooka to regulate apical membrane differentiation. Our results reveal an important functional link between Pak4, AJ material morphogenesis, and polarity remodeling during organogenesis downstream of Par3.

INTRODUCTION

In vertebrate and invertebrate epithelial or neuroepithelial cells, apical membrane morphogenesis consists of the differentiation of the cell-cell junction (zonula adherens [ZA]) from the apical and lateral membrane domains. How this is achieved is not fully understood. In *Drosophila*, apical membrane morphogenesis and remodeling requires at least two processes: (1) the confinement of the conserved polarity proteins Par6-atypical protein kinase C (aPKC), Crumbs (Crb), and Stardust (Sdt) to the apical pole of the cell and (2) the exclusion of Baz (*Drosophila* Par3) from the apical membrane, such that this protein is positioned at the boundary between the apical and lateral membrane where the ZA assembles (Krahn et al., 2010; Morais-de-Sá et al., 2010; Walther and Pichaud, 2010). These two processes drive polarity specification and remodeling in the follicular epithelium, the cellularizing blastoderm, and the photoreceptor (St Johnston and Ahringer, 2010). Notably, the junctional configuration and localization of the apical proteins Par6-aPKC and Baz/Par3 relative to the apical-lateral border is conserved through evolution (Afonso and Henrique, 2006; Totong et al., 2007; Zihni et al., 2014).

In addition to the apical exclusion of Baz, and in order to limit apical membrane morphogenesis to one pole of the cell, Baz must be excluded from the lateral cortex. Lateral exclusion of Baz prevents its ectopic association with aPKC basal to the ZA and is mediated by the serine/threonine kinase Par1 in several model epithelial cell types (Benton and St Johnston, 2003b). However, the relatively mild *par1* loss-of-function polarity phenotype observed in the follicular epithelium, blastoderm, and photoreceptor suggests that other mechanisms might be at play (Benton and St Johnston, 2003b; McKinley and Harris, 2012; Nam et al., 2007). For example, in the blastoderm where polarity is established de novo, basal to apical transport of Baz and the presence of an apical scaffold of F-actin can act to localize Baz at the apical pole of the cortex (Harris and Peifer, 2004; McKinley and Harris, 2012). Whether these or other mechanisms regulate the ZA localization of Baz in a remodeling epithelium is not clear.

As Baz is confined to the apico-lateral border of the cell, it is thought to interact with adherens junction (AJ) material, possibly via binding to Arm and Echinoid (Wei et al., 2005). However, in the blastoderm, follicular epithelium, or photoreceptor, accumulation of AJ material at the plasma membrane does not strictly depend on Baz (Harris and Peifer, 2004; Shahab et al., 2015; Walther and Pichaud, 2010). This indicates that pathways must promote AJ assembly independently of *baz*. These pathways and their relation to the epithelial polarity gene network remain to be characterized in detail.

Among the factors that might regulate AJ morphogenesis is the Cdc42 effector P21-activated serine/threonine kinase, Pak4 (*Drosophila mushroom bodies tiny* [*mbt*]). In *Drosophila* photoreceptors, this kinase localizes at the developing ZA and is required for proper ZA morphogenesis (Schneeberger and Raabe, 2003). In addition, Mbt can phosphorylate β-cat/Arm in vitro, and in cell culture, this phosphorylation limits the association of Arm and E-cadherin (Menzel et al., 2008). Consistent with a conserved role for Mbt/Pak4 in regulating AJ morphogenesis, conditional deletion of mPak4 in the mouse nervous system leads to a loss of neuroepithelial AJs (Tian et al., 2011). In addition, hPak4 is required to promote tight junction and AJ maturation in human bronchial cells (Wallace et al., 2010). Thus, Pak4/Mbt plays an important role in regulating epithelial polarity across phyla. However, the functional relationship between this kinase, AJ morphogenesis, and the conserved epithelial polarity gene network remains to be examined in detail.

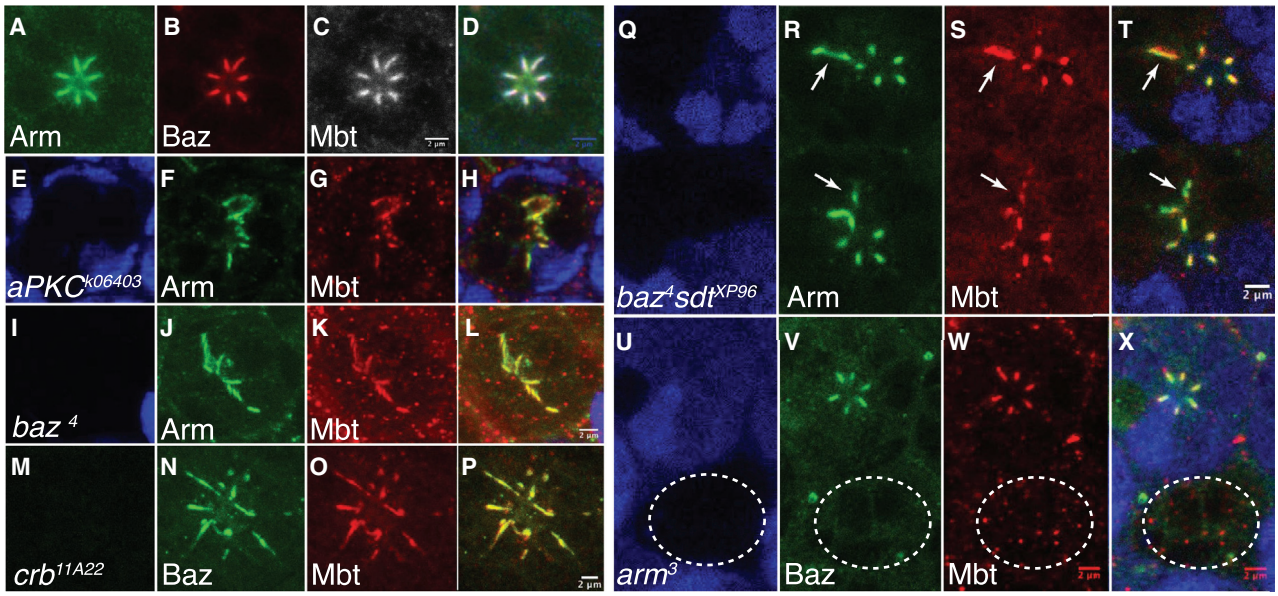

Figure 1. Mbt Is a Core Component of the AJ

(A–D) Wild-type ommatidium. Arm (green; A), Baz (red; B), Mbt (gray; C), and merge (D) are shown.
(E–H) *aPKC*^{k06403} *mutant*, lacking GFP (blue; E), Arm (green; F), Mbt (red; G), and merge (H).
(I–L) *baz*^{4} mutant, lacking GFP (blue; I), Arm (green; J), and Mbt (red; K), and merge (L).
(M–P) *crb*^{11A22} mutant, lacking GFP (blue; M), Baz (green; N), Mbt (red; O), and merge (P).
(Q–T) *baz*^{4}, *sdt*^{XP96} mutant, lacking GFP (blue; Q), Arm (green; R), Mbt (red; S), and merge (T). White arrows point to mutant cell-cell interfaces.
(U–X) *arm*^{3} *mutant*, lacking GFP (blue; U), Baz (green; V), Mbt (red; W), and merge (X). A mutant ommatidium is circled.
The scale bars represent 2 μm.

RESULTS

Baz Is Essential for Photoreceptor Polarity Remodeling

The *Drosophila* photoreceptor, which undergoes a sustained phase of apico-basal polarity remodeling during development, is a particularly attractive model to study the relationship between the conserved polarity determinants and the AJ during cortical polarity remodeling and plasma membrane morphogenesis (Figure S1A).

In light of recent work suggesting that *baz* might be dispensable in some instances of epithelial polarity remodeling in vivo (Shahab et al., 2015), we first re-examined the function of this factor in the remodeling photoreceptor using two new loss-of-function alleles: *baz*^{XR11} *and baz*^{EH747}. Both alleles lead to a strong reduction in aPKC, Crb, and Par6 staining (Figures S1A–S1J). In addition, most mutant photoreceptors fail to specify a clear ZA and AJ material invades what would normally be the apical pole of the cell (Figure S1E). These data confirm that Baz is required to support the recruitment of Par6-aPKC and Crb at the apical cortex and membrane, respectively (Walther and Pichaud, 2010). However, we note instances where the ZA is relatively well defined (Figure S1I). These instances correlate with residual apical Par6 accumulation (Figure S1H), which suggests that Par6 can be recruited at the apical pole of the cell independently of Baz, presumably through binding to Cdc42 or Crb (Hutterer et al., 2004; Morais-de-Sá et al., 2010).

Mbt Is a Core Component of the AJ

In the developing photoreceptor, Mbt localizes at the developing ZA (Schneeberger and Raabe, 2003; Figures 1A–1D). To test whether this localization depends on the apical epithelial gene network, we examined Mbt localization in *aPKC*^{k06403} (Figures 1E–1H), *baz*^{4} (Figures 1I–1L), *crb*^{11A22} (Figures 1M–1P), and *baz*^{4}, *sdt*^{XP96} double-mutant cells (Figures 1Q–1T). We found that AJ domains, which contain Mbt, are still present in all these conditions. The only condition that abolishes Mbt localization at the cell cortex is in *arm*^{3} mutant cells, where AJ material is absent (Figures 1U–1X).

From this set of data, we can therefore draw two main conclusions. First, Mbt is a core component of the AJ. Second, there must be at least one molecular pathway that can support AJ assembly independently of Baz and Crb. Due to its close association with AJ material, we reasoned that Mbt could be part of such pathway. To test this possibility, we generated *baz*^{4}, *mbt*^{P1} double-mutant cells and compared them to *baz*^{4} and *mbt* ^{P1} single-mutant cells. AJ material is detected in *baz*^{4} (Figure S1E) and in *mbt*^{P1} single-mutant photoreceptors (Figure 2A–D). In contrast, we found that no AJ material can be detected at the cortex of *baz*^{4}, *mbt*^{P1} double-mutant cells (Figures 2K–2N). Therefore, our results indicate that *mbt* can support AJ morphogenesis independently of *baz*.

Mbt Supports AJ Morphogenesis Independently of *baz*

Next, we sought to examine the role of *mbt* during photoreceptor polarity remodeling. Consistent with Mbt promoting ZA

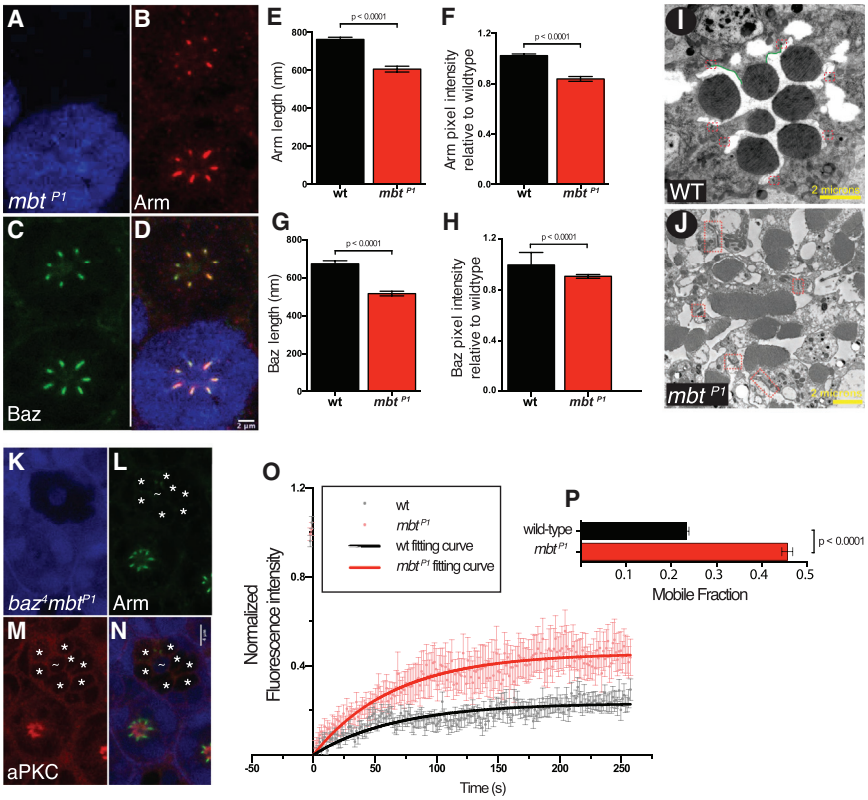

Figure 2. *mbt* Promotes AJ Morphogenesis Independently from Baz

(A–D) mbt^{P1} mutant, lacking GFP (blue; A), Arm (red; B), Baz (green; C), and merge (D). The scale bars represent 2 microns.

(E) Mean length of Arm cortical domain in wild-type and mbt^{P1} mutants.

(F) Mean pixel intensity of Arm in wild-type and mbt^{P1}. In (E) and (F), n = 202 (in four wild-type retinas) and n = 460 (in four mbt^{P1} retinas).

(G) Mean length of Baz cortical domain in wild-type and mbt^{P1} mutants.

(H) Mean pixel intensity of Baz in wild-type and mbt^{P1}. In both (G) and (H), n = 99 (wild-type) and n = 107 (mbt^{P1}), with measurements taken from five independent mbt^{P1} mosaic retina. In (E)–(H), columns represent mean and error bars represent the SEM of each dataset. Statistical significance was determined using an unpaired two-tailed Student's t test.

(I and J) Electron microscopy (I) on a wild-type ommatidium and (J) on the poorly developed apical membranes of an mbt^{P1} adult ommatidium. Ectopic AJ domains are boxed and sub-apical membranes in green. The scale bar represents 2 μm.

(K–N) baz^4, mbt^{P1} mutant lacking GFP (blue; K), Arm (green; L), aPKC (red; M), and merge (N). Asterisks highlight mutant cells. A tilde marks a wild-type cell. The scale bars represent 4 μm.

(O) FRAP on E-cadherin::GFP in wild-type or mbt^{P1}. Mean normalized fluorescence intensity in wild-type (gray; n = 18 from two individuals) and mbt^{P1} (pink; n = 15 from three individuals) is shown; error bars represent SEM. Fluorescence recovery curves of E-cad::GFP after photo-bleaching in wild-type (black) and mbt^{P1} (red) are shown.

(P) Mobile fraction of E-cadherin::GFP in a wild-type (black) or mbt^{P1} (red) background. The p value was calculated with an unpaired two-tailed Student's t test with Welch's correction.

morphogenesis, we measure a significant decrease in the length and mean pixel intensity of Arm and Baz at the developing ZA of mbt^{P1} mutant photoreceptors (Figures 2A–2H). In addition, *mbt* is required for overall apical membrane differentiation, albeit only in a fraction of the mutant cells (Figures 2I and 2J). We found that, in 40% of the mbt^{P1} mutant ommatidia (n = 2,662 from nine retinae), no ZA assembles along the photoreceptors proximo-distal axis, and instead, poorly differentiated apical membranes are found between the floor of the retina and the lamina part of the brain (Figures 2J and S2A–S2J). Whereas these membranes contain aPKC, Crb, Baz, and Arm, apico-basal polarity is severely compromised (Figures S2D–S2G''). These data indicate that Mbt promotes AJ morphogenesis and to some extent apical membrane morphogenesis. Importantly, the *mbt* phenotype can be fully rescued when expressing a wild-type version of this kinase (Figure S3A). In contrast, re-introducing a version of Mbt that can no longer bind to Cdc42 or lacks kinase activity (Schneeberger and Raabe, 2003) fails to rescue the *mbt* phenotype (Figure S3A). Therefore, Mbt functions through its kinase activity, which, as expected for this family of kinases, is regulated via binding to Cdc42 (Ha et al., 2015).

Mbt Does Not Phosphorylate Par6 in *Drosophila*

In order to gain mechanical insight into how Mbt might regulate apical membrane morphogenesis, we examined the relationship between Mbt and Par6. Human Pak4 (hPak4) can phosphorylate hPar6b at serine 143, which is found in *Drosophila* Par6 at position 146 (Jin et al., 2015). However, the (−2) residue in Par6 differs from that found in hPar6b, and in that, Par6 most resembles hPar6a, which is not phosphorylated by hPak4 (Figures S3B and S3C).

To test whether Mbt can phosphorylate Par6, we purified an activated version of Mbt from S2 cells and used it to perform kinase assays with *Drosophila* Par6. In our assays, we found no evidence for Mbt (or for recombinant hPak4) phosphorylating Par6S146 in vitro (Figures S3D and S3E). In addition, a version of Par6 in which S146 is mutated to an alanine (Par6-Par6SA146) can rescue the embryonic lethality of the $par6^{\Delta 226}$ when expressed under the *par6* promoter (data not shown). Thus, our results indicate that phosphorylation of Par6S146 is not essential for Par6 function during *Drosophila* development.

Mbt Regulates the Stability of E-cadherin at the ZA

Mbt influences the stability of the E-cadherin-catenin complex in non-polarized S2 cells (Menzel et al., 2008). To examine whether this contributes to regulating ZA morphogenesis, we made use of fluorescence recovery after photobleaching (FRAP) to evaluate the mobile fraction and half-time recovery of E-cadherin. When photobleaching the basal tip of the wild-type ZA, we find that 23.3% ± 0.6% of E-cadherin::GFP is mobile with an evaluated

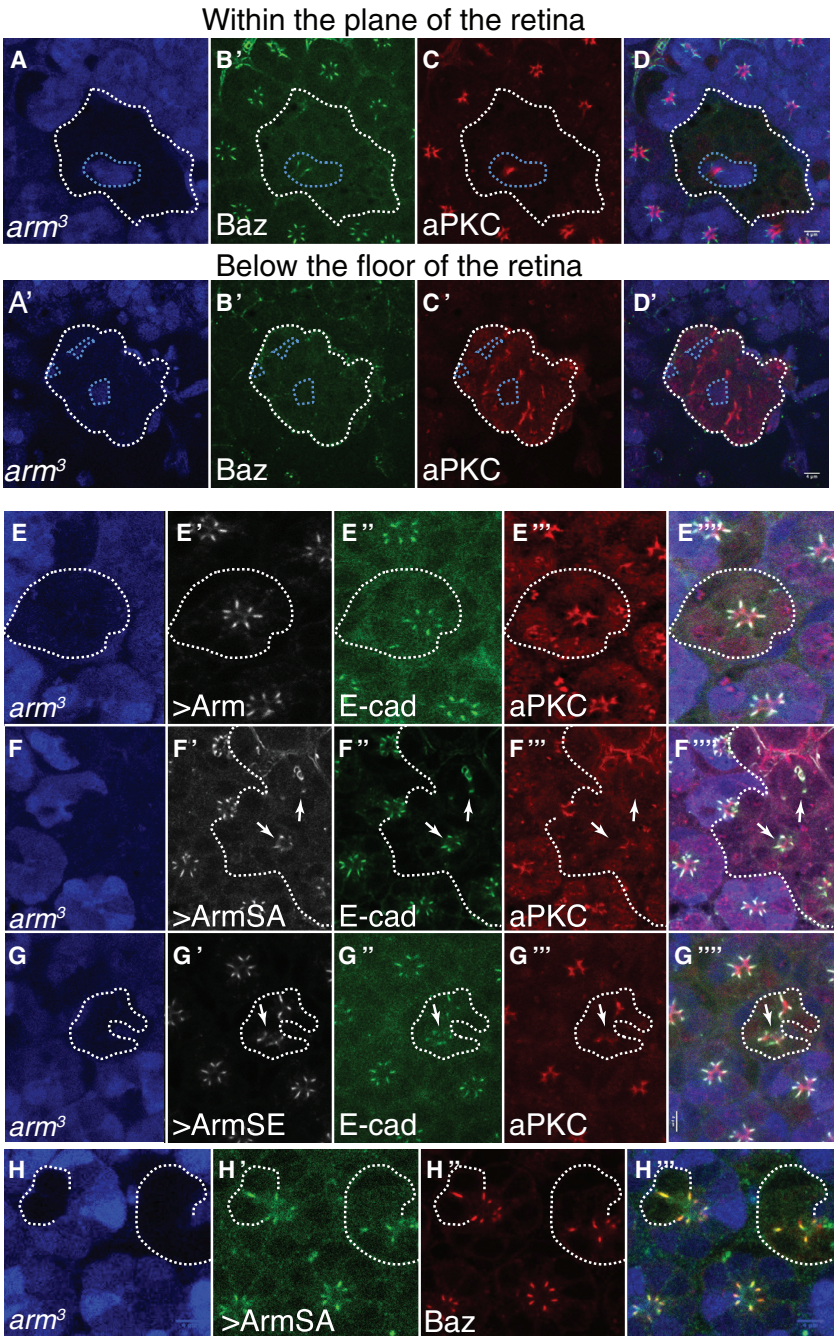

Figure 3. *mbt* Regulates ZA Remodeling through Arm Phosphorylation

(A–D') *arm*^{3} mutant, lacking GFP (blue; A and A'), Baz (green; B and B'), aPKC (red; C and C'), and merge (D and D').

(E–G'''') Myc (gray), E-cadherin (green), aPKC (red). (E–E'''') Rescue of an *arm*^{3} mutant ommatidium, lacking GFP (blue; E), by re-introduction of a wild-type version of the Arm::Myc transgene is shown. (F–F'''') Re-introduction of ArmSA561,688::Myc is shown. (G–G'''') Re-introduction of ArmSE561,688::Myc is shown.

(H–H''') *arm*^{3} mutant lacking GFP (blue; H), ArmSA561,688::Myc (green; H'), Baz (red; H''), and merge (H''').

The scale bars represent 4 μm.

half-time recovery of 47 s (Figures 2O and 2P). In *mbt*^{P1} mutant ZA, we found that the mobile fraction of E-cadherin::GFP is 45.7% ± 1.2% with a half-time recovery of approximately 45 s (Figures 2O and 2P). Therefore, Mbt is required to stabilize E-cadherin at the ZA during photoreceptor polarity remodeling.

Mbt Regulates ZA Remodeling through Arm Phosphorylation

Phosphorylation of β-cat/Arm by Pak4/Mbt is conserved through evolution (Selamat et al., 2015), thus providing a potential mechanism for regulating AJ morphogenesis and E-cadherin mobility. Therefore, we next sought to re-examine the relationship between Mbt, Arm phosphorylation, and ZA morphogenesis. First, we confirmed that a constitutively active form of Mbt phosphorylates Arm at S561 and S688 (Figures S3D and S3E). Second, we generated transgenic animals bearing myc-tagged phospho-mimetic (*UAS-armSE561,688::myc*), phospho-dead (*UAS-armSA561,688::myc*), and wild-type (*UAS-arm::myc*) transgenes and asked whether these could rescue the *arm*^{3} mutant phenotype. *arm*^{3} mutant photoreceptors show defects in aPKC localization at their cortex, lack Baz altogether, and, similar to *mbt* mutant cells, tend to form cysts below the floor of the retina (Figures 3A–3D').

Re-introducing Arm::myc in *arm*^{3} mutant cells rescues the photoreceptor polarity remodeling phenotype (Figure 3E). However, re-introducing either ArmSA561,688::myc or ArmSE561,688::myc in *arm*^{3} mutant photoreceptors fails to support ZA morphogenesis, and instead, discrete AJ domains are found distributed along the proximo-distal axis of the cell. Both transgenes are able to form domains that contain E-cadherin and Baz (Figures 3F–3H). In the case of ArmSA561,688::myc, two of the ZA-like domains examined (n = 24) present ArmSA561,688::myc, but lack Baz entirely. Among the remaining 22 ZA-like domains, four include a region positive for ArmSA561,688::myc, but not Baz, and three include regions positive for Baz, but not ArmSA561,688::myc. These results suggest that the phosphorylation status of Arm regulates the interface between the AJ and Baz. In addition, we note that, with ArmSA561,688, several cells present poorly differentiated apical membranes including aPKC domains that are smaller than in the wild-type (Figures 3F'''–3G''' and S4).

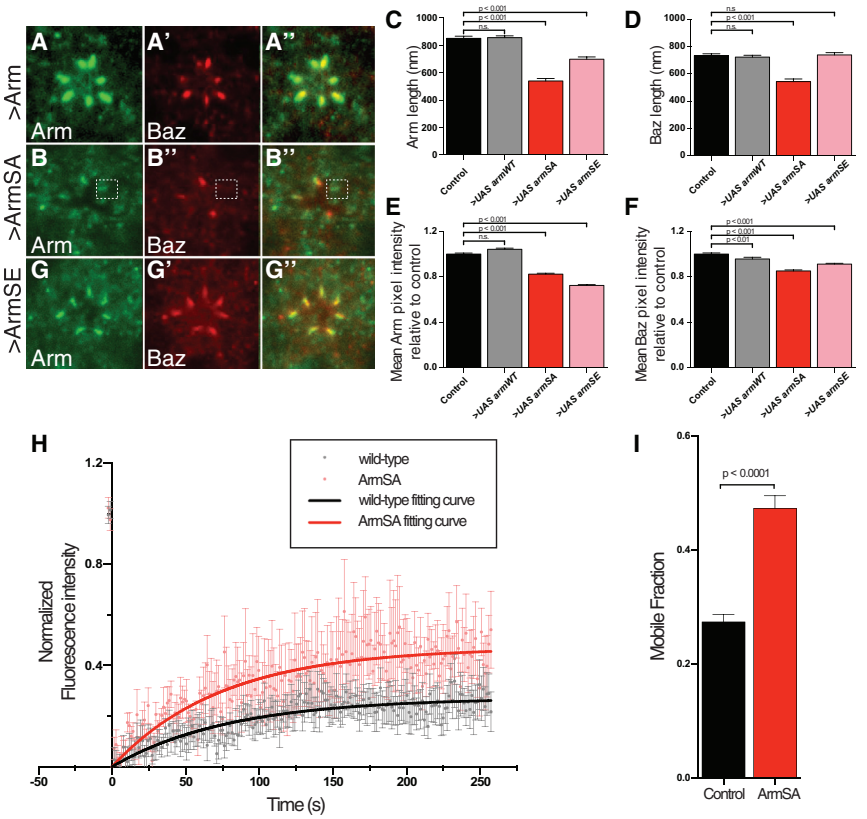

Figure 4. Arm Phosphorylation Regulates AJ Material Stability during ZA Morphogenesis

(A) Overexpression of Arm::myc. Arm (green) and Baz (red) are shown.

(B) Overexpression of ArmSA561,688::myc. Arm (green) and Baz (red) are shown. A dashed rectangle highlights a ZA that contains Arm, but not Baz.

(C and D) Length of the Arm (C) and Baz (D) domains in wild-type and in photoreceptors expressing Arm::myc, ArmSA561,688::myc, or ArmSE561,688::myc.

(E and F) Mean pixel intensity for Arm (E) and Baz (F) measured relative to that of control photoreceptors. In (C)–(F), columns indicate the mean whereas error bars indicate the SEM (n > 200). Statistical significance was determined using one-way ANOVA and the Kruskal-Wallis multiple comparison test for non-parametric samples.

(G–G'') Overexpression of ArmSE561,688::myc; Arm (green; G), Baz (red; G'), and merge (G'').

(H) FRAP on E-cadherin::GFP in wild-type cells and in cells expressing ArmSA561,688::myc. Mean normalized fluorescence intensity in wild-type (gray; n = 14 from five individuals) and ArmSA561,688::myc (red; n = 9 from five individuals) is shown. Error bars represent SEM. Fluorescence recovery curves of E-cadherin::GFP after photo-bleaching in wild-type (black) and ArmSA561,688::myc (red) are shown.

(I) Mobile fraction of E-cadherin::GFP in a wild-type (black) or ArmSA561,688::myc (red) background. The p value was calculated with an unpaired two-tailed Student's t test with Welch's correction.

Altogether, our results indicate that the developing ZA influences apical membrane differentiation. They also suggest that the fraction of phosphorylated Arm must be present in the correct proportion to support ZA morphogenesis. This notion is further supported by the fact that expressing an activated form of Mbt is detrimental to photoreceptor polarity remodeling and ZA maturation (Figures S3G–S3I).

Arm Phosphorylation Promotes the Accumulation of AJ Material at the ZA

If Arm phosphorylation must be finely tuned during ZA remodeling, then overexpressing ArmSA561,688 should lead to phenotypes resembling that of the *mbt* loss of function. To test this hypothesis, we overexpressed ArmSA561,688::myc in wild-type retinae. In this assay, overexpressing wild-type Arm::myc does not lead to significant phenotypes (Figures 4A, 4C–4F, and S4A). In contrast, overexpressing ArmSA561,688::myc leads to a decrease in Arm and Baz as well as a significant shortening of the ZA when compared to wild-type (Figures 4C–4F). We also note instances where Baz is missing from the ZA, while Arm is present (Figure 4B). This is specific, as expressing ArmSE561,688::myc or Arm::myc does not lead to such uncoupling between Arm and Baz (Figures 4A, 4G, S4C, and S4E). Expressing the ArmSE561,688::myc transgene leads to a significant decrease in length and mean pixel intensity for Arm. In this case, however, the length of the Baz domain is comparable to wild-type (Figure 4D). Finally, when overexpressing the ArmSA561,688::myc transgene, the mobile fraction for E-cadherin::GFP determined using FRAP is 47% ± 2.2% (Figures 4H and 4I), which is almost identical to that we measured in *mbt* mutant cells (Figures 2O and 2P). Altogether, the range of phenotypes we obtained when overexpressing ArmSA561,688::myc is similar to that seen in *mbt* mutant photoreceptors. These data therefore support a model in which Mbt regulates the stability of E-cadherin at the membrane as well as the cortical accumulation of Arm and Baz through phosphorylation of Arm at serine 561 and 688.

Mbt Promotes the Retention of Baz at the Developing ZA

Next, we sought to probe the relationship between *mbt*, ZA morphogenesis, and Baz localization. Our results so far suggest a model in which *mbt* might promote the retention of Baz at the developing ZA. To test this model, we overexpressed a wild-type version of Baz (Baz::GFP) in *mbt* mutant cells and tested for the presence of ectopic accumulation of Baz::GFP at the lateral cortex of the photoreceptors. Baz::GFP expressed in an otherwise wild-type retina localizes at the ZA in 98% of photoreceptors quantified (n = 528; Figures 5A and 5E). In contrast, expressing Baz::GFP in *mbt* mutant cells leads to the formation of Baz::GFP microdomains in 33% of the lateral cortices examined (n = 231; Figures 5B and 5E). These lateral cortices can contain up to three ectopic Baz domains that also contain aPKC and

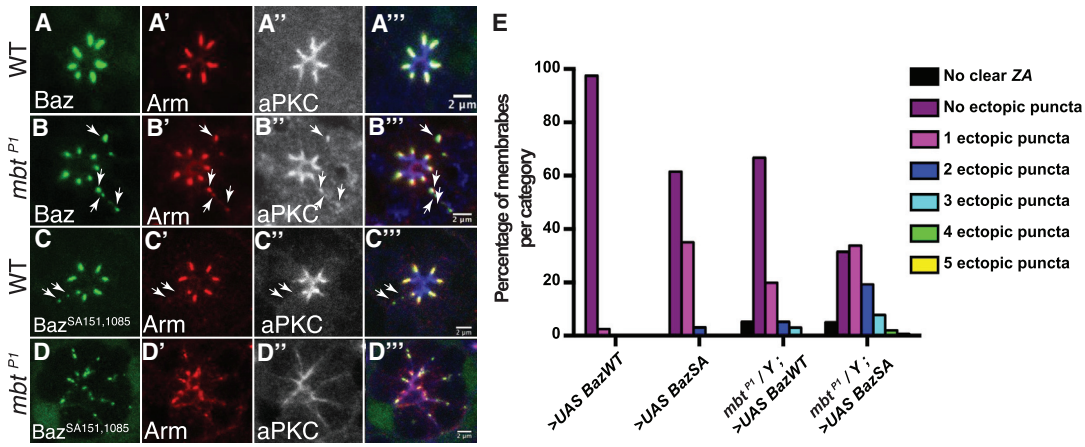

Figure 5. Mbt Promotes Baz Retention at the Developing ZA

(A–A''') Baz::GFP (green; A) in a wild-type ommatidium. Arm (red, A'), aPKC (gray; A''), merge (A'''). Note that the aPKC channel is in blue in the merged panel.

(B–B''') Expression of Baz::GFP (green; B) in an mbt^{P1} ommatidium. Arm (red, B'), aPKC (gray; B''), merge (B'''). Note that the aPKC channel is in blue in the merged panel. White arrows point to ectopic Baz aggregates.

(C–C''') Expression of BazSA151,1085::GFP (green; C) in a wild-type ommatidium. Arm (red; C') aPKC (gray; C''), merge (C'''). Note that the aPKC channel is in blue in the merged panel. White arrows point to ectopic Baz aggregates.

(D–D''') Expression of BazSA151,1085::GFP (green; D) in an mbt^{P1} mutant. Arm (red; D'), aPKC (gray; D''), merge (D'''). Note that the aPKC channel is in blue in the merged panel. The scale bar represents 2 μm.

(E) Quantification of the number of GFP puncta at the photoreceptor lateral membranes. On the x axis, BazSA stands for BazSA151,1085.

Arm. In addition, up to 88% of the ommatidia (n = 1,286 from four retinae) present poorly developed apical membranes compared to 40% in the case of mbt^{P1} (n = 2,662 from nine retinae). These data demonstrate that *mbt* limits the ability of Baz to form microdomains at the photoreceptor lateral cortex. They also provide a genetic link between *mbt*, the developing ZA and *baz*, indicating that a defect in ZA retention of Baz leads to the ectopic recruitment of aPKC and Arm at the lateral membrane.

Mbt and Par1 Function Redundantly to Prevent Baz Accumulation at the Lateral Cortex

A requirement for *mbt* in preventing Baz from accumulating at the lateral cortex raises the issue that the function of Mbt might be related to that of Par1. During polarity remodeling, Par1 expression is restricted to the lateral cortex of the photoreceptor (Figures S5A and S5B). In addition, expressing a Par1 transgene that escapes aPKC phosphorylation (Par1[AEM]::GFP) leads to its ectopic localization at the apical membrane (Doerflinger et al., 2010), thus indicating that apical exclusion of Par1 is mediated by aPKC phosphorylation (Figures S5C and S5D). Therefore, the localization pattern of Par1 is consistent with this kinase promoting lateral exclusion of Baz. In addition, similar to the developing follicular epithelium (Doerflinger et al., 2010), we measure an increase in the quantity of microtubules present in the soma of *par1* mutant photoreceptors (Figures S5E and S5F).

Quantifications performed on mature photoreceptors show that the *par1* loss-of-function polarity phenotype is very mild and consists of cells that present slightly longer sub-apical membranes (Figures S5G–S5J). Such a mild phenotype might be due to the presence of other redundant kinases phosphorylating Baz at serines 151 and 1085. In order to bypass such possible redundancy, we made use of the BazSA151,1085::GFP transgene (Benton and St Johnston, 2003b). Expressing this fusion protein in a wild-type retina leads to the formation of at least one ectopic BazSA151,1085::GFP microdomain in 35% of photoreceptor lateral cortices (n = 734; Figures 5C and 5E). However, BazSA151,1085::GFP is localized exclusively at the developing ZA in the majority (65%) of photoreceptors and ZA localization is observed when expressed in baz^4 mutant cells, which rules out a recruitment of BazSA151,1085::GFP via Baz oligomerization (Benton and St Johnston, 2003a; Figure S5K). From these experiments, we conclude that *par1*-dependent lateral exclusion of Baz is largely dispensable during photoreceptor polarity remodeling.

To test whether *mbt* functions redundantly with *par1*, we expressed BazSA151,1085::GFP in *mbt* mutant photoreceptors. In this condition, we observe an extensive ectopic localization of BazSA151,1085::GFP with lateral cortices containing up to five ectopic domains (n = 296; Figures 5D and 5E). This is accompanied by a very severe polarity phenotype, in that the aPKC and Arm expression domains extend laterally.

Altogether, these results indicate that Mbt-dependent ZA retention of Baz constitutes a main localization mechanism for this factor. This retention mechanism operates together with Par1-dependent lateral exclusion. Importantly, failure to limit Baz localization at the developing ZA leads to catastrophic defects during polarity remodeling.

DISCUSSION

Mbt Regulates the Accumulation of AJ Material at the Developing ZA

In the developing pupal photoreceptor and other popular model-developing epithelial cell types, the concomitant apical exclusion

of Baz and accumulation of Crb promotes the coalescence of AJ material during ZA remodeling (St Johnston and Ahringer, 2010). However, how AJ morphogenesis is regulated at the plasma membrane is not well understood. Here, we present complementary evidence indicating that Pak4/Mbt regulates this process. In the absence of *mbt* and when compared to wild-type cells, we measure less Arm at the ZA. The AJ domains that we observe in *baz* (or *baz*, *sdt*) mutant photoreceptors are no longer detected when *mbt* is also lacking. In addition, our FRAP experiments indicate that *mbt* limits the amount of E-cadherin::GFP that can be recovered at the remodeling ZA. Finally, expressing a version of Arm that cannot be phosphorylated by Mbt leads to a shortening of the ZA and a decrease in Baz levels similar to that measured in *mbt* mutant cells. The mobility that we measured for E-cadherin in these shorter ZA is comparable to that measured in *mbt* mutant cells. Therefore, our results indicate that, in vivo, Mbt promotes AJ morphogenesis at least in part through phosphorylation of Arm S561 and S688.

Mbt Function Is Linked to Arm Phosphorylation

Residues S561 and S688 are located in a domain of Arm that mediates part of the E-cadherin-catenin interface. Their phosphorylation destabilizes the E-cadherin-catenin interaction and cell-cell adhesion in non-polarized S2 cells (Menzel et al., 2008). Therefore, loss of *mbt* should lead to a stabilization of the E-cadherin-catenin interaction. We find that, at the developing photoreceptor ZA, loss of *mbt* promotes E-cadherin mobility as well as a decrease in Arm and Baz content. As E-cadherin is coupled to Arm, it also becomes coupled to the underlying F-actin cortex, which might influence AJ motility. Interestingly, Pak4/Mbt has been shown to promote the phosphorylation of the F-actin-severing protein cofilin at the conserved Ser3 (Dan et al., 2001; Menzel et al., 2007). Phosphorylation of cofilin inactivates it and leads to a slowing down of F-actin turnover (Bravo-Cordero et al., 2013). Reduced turnover of cortical F-actin has been associated with the stabilization of E-cadherin trans-interactions in vitro (Engl et al., 2014). We therefore propose that, upon loss of *mbt*, stabilization of the E-cadherin-catenin interface, perhaps combined with increased cofilin-dependent F-actin turnover, directs E-cadherin mobility. Altogether, our results indicate that the dynamic regulation of the E-cadherin-catenin interaction is important for ZA morphogenesis.

ZA Retention of Baz Is Required for Proper Apical Membrane Differentiation

In the remodeling photoreceptor, Baz, Par6, aPKC, and Crb all overlap with the apical 2/3 of the ZA, whereas the basal 1/3 presents very little staining for these proteins (Walther and Pichaud, 2010). In addition, we show here that the expression domain of Par1 abuts the basal boundary of the ZA. Therefore, the basal 1/3 of the developing ZA, which is approximately 350 nm in length, allows for a clear spatial separation of Baz and Par1 at the cortex. In *mbt* mutant cells, the length of the developing ZA along the apico-basal axis is significantly reduced, which largely abolishes this clear separation and might expose Baz to Par1 phosphorylation and promote its cortical exclusion. This might explain why we detect less Baz at the ZA of *mbt* mutant photoreceptors. In this model, Mbt would antagonize Par1 so to maintain an optimum pool of Baz at the ZA. Alternatively, a failure in retaining Baz at the ZA might lead to its ectopic localization at the lateral membrane, where it is targeted by Par1. In this second model, ZA retention and Par1 lateral exclusion of Baz function redundantly. This second model is supported by our finding that, when overexpressed in *mbt* mutant cells, Baz-SA151,1085::GFP accumulates at the lateral membrane. In any case, we find that Mbt-dependent AJ material accumulation influences apical membrane morphogenesis, and our genetic experiments indicate that this is through promoting the retention of Baz at the ZA. We note that both ArmSA561,688 and ArmSE561,688 support the recruitment of Baz at the developing ZA in rescue experiments. Thus, the phosphorylation status of Arm does not directly influence Baz recruitment at the ZA.

In vertebrate epithelial cells as well as in the photoreceptor, Pak4 functions downstream of the small GTPase Cdc42, which also regulates the Par6-aPKC module (Schneeberger and Raabe, 2003; Wallace et al., 2010; Walther and Pichaud, 2010). Therefore, our finding that Pak4 promotes the accumulation of Baz, a factor required for the accumulation of Par6-aPKC at the apical membrane, reveals an important functional cross-talk between AJ morphogenesis and apical membrane differentiation during polarity remodeling.

EXPERIMENTAL PROCEDURES

Antibodies and Immunological Methods

Whole-mount retinae were prepared as described in Walther and Pichaud (2006). The following antibodies were used: mouse anti-alpha tubulin 1/1,000 (Sigma); rabbit anti-PKCζ 1/200 (Santa Cruz Biotechnology); mouse anti-Arm 1/200 (N27-A1; Developmental Studies Hybridoma Bank); rabbit anti-Baz 1/2,000 (generated against C-terminal peptide H2N - CSQ YGS AAG SQP HAS KV - COOH; this work; Eurogentec SA); rat anti-Crb 1/200 (generated against C-terminal peptide H2N - H2N - CEM DNV LKP PPE ERL I - COOH; this work; Eurogentec SA); rat anti-E-cadherin 1/50 (DCAD2; Developmental Studies Hybridoma Bank); guinea pig anti-Mbt 1/200 (generated against peptides H2N - SSN RPLPLVDPSEIT C-CONH2 and H2N-PHHNNNKADTTSLNSC-CONH2; this work; Eurogentec SA); mouse anti-Myc 1/50 (9E10; Developmental Studies Hybridoma Bank); rabbit anti-Par1 1/200 (McDonald et al., 2008); guinea pig anti-D-Patj 1/400 (generated against C-terminal peptide H2N - SAS MGA EPD LIP DWR N - COOH; this work; Eurogentec SA); guinea pig anti-Par6 1/1000 (generated against C-terminal peptide H2N - CHH QQA ASN AST IMA SDV KDG VLH L - COOH; this work; Eurogentec SA); and rabbit anti-Sdt 1/250 (Berger et al., 2007), with the appropriate combination of mouse, guinea pig, rabbit, and rat secondary antibodies conjugated to Dy405, Alexa 488, Cy3, or Cy5 as appropriate at 1/200 each (Jackson ImmunoResearch). Retinae were mounted in VectaShield, and imaging was performed using a Leica SP5 confocal. Images were edited using ImageJ and Adobe Photoshop 7.0.

Fluorescent Recovery after Photobleaching

Pupal retinas were mounted at 40% after puparium formation (APF) by removing the pupal cuticle and carefully exposing the retina. Live imaging was performed on a Leica SP5 confocal with a 63× 1.4 numerical aperture (NA) oil immersion objective and the following settings: pixel resolution 512 × 512; speed 400 Hz; 10% 488-nm laser power at 20% argon laser intensity; and 5× zoom. The basal tip of the AJ was marked with a five-pixel-diameter circle region of interest (ROI) and photo-bleached with a single pulse using 90% 488-nm laser power at 20% argon laser intensity. AJ recovery was recorded every 1.293 s with the previously mentioned settings for 200 frames (E-cadherin::GFP).

Statistical Analyses

Length and pixel intensity measurements of Baz and Arm were determined by analyzing confocal images of *mbt* mosaic retina at 40% APF. For

quantification of Baz and Arm length and intensity in retina expressing Arm::myc, ArmSA561,688::myc and ArmSE561,688::myc images were acquired from samples processed simultaneously, using ubi-E-cadherin::GFP retinae as an internal control. In all cases, a threshold was applied to the original data files and then both the length of the Baz- or Arm-positive domain and the mean pixel intensity along this line were measured using the line tool in Fiji (Schindelin et al., 2012). To correct for differences in pixel intensity between retinas of the same genotype within an experiment, the measured average pixel intensity of signal of all junctions in control samples was determined. All individual pixel intensity measurements were then divided by this constant to determine the mean pixel intensity relative to control. In all cases, at least four independent retinae were used for each genotype and matched control.

Mean pixel intensity and area of α-tubulin immunofluorescence in wild-type and $par1^{D16}$ mutant ommatidia were determined by analyzing confocal images of $par1^{D16}$ mosaic retinae at 40% APF. A total of nine confocal images in which a wild-type ommatidium was found adjacent to an ommatidium fully mutant for $par1^{D16}$ were selected for analysis in Fiji. A threshold was applied to the α-tubulin channel and then the wand (tracing) tool was used to specify the regions of α-tubulin staining in wild-type and mutant tissue. The mean intensity and the total area of these paired regions were determined using the measure tool. This method was also used to quantify aPKC immunofluorescence in arm^{3} mutant ommatidia expressing ArmSA561,688.

To determine the percentage of ommatidia below the retinal floor, retinae of the indicated genotypes were dissected at 40% APF. Immunostaining was performed using antibodies against aPKC and Arm to mark the apical membrane and ZA, respectively. Confocal images of each whole retina were acquired, with z-sections taken at two microns intervals. Retinae were manually scored to determine the percentage of ommatidia with aPKC- and Arm-positive membrane domains below the retinal floor. A minimum of four retinae were scored for each genotype. Because in the genotype mbt^{P1}/Y ; *GMR-Gal4/UAS-*mbt^{KD} a proportion of ommatidia found below the retinal floor contained neither apical membrane nor ZA markers, for this genotype, the analysis was repeated using antibodies against E-cadherin, aPKC, and NaK (mouse a5 antibody; 1/50; Developmental Studies Hybridoma Bank [DSHB]) to mark the cell membrane.

For quantification of Baz::GFP puncta, the total number of ectopic Baz::GFP puncta was quantified in the following genotypes: (1) ; *GMR-Gal4/UAS-baz::GFP* ; (2) ; *GMR-Gal4/UAS-bazSA151,1085::GFP* ; (3) mbt^{P1}/Y ; *GMR-Gal4/UAS-baz::GFP* ; and (4) mbt^{P1}/Y ; *GMR-Gal4/UAS-bazSA151,1085::GFP;*. For each genotype, at least 230 cell interfaces from a minimum of five independent retinas were quantified. In all genotypes, it was assumed that one of the GFP-positive puncta scored corresponded to the ZA. All data were tested for normality with the D'Agostino-Pearson test. Parametric samples were tested for statistical significance using an unpaired two-tailed Student's t test. Nonparametric samples were tested for statistical significance using an unpaired two-tailed Mann-Whitney test. For experiments consisting of more than one experimental condition, statistical significance was determined with one-way ANOVA and Dunnett's multiple comparison test or the Kruskal-Wallis multiple comparison test for parametric or non-parametric samples, respectively. For the measurement of α-tubulin and aPKC, mean pixel intensity, and area, statistical significance was determined using the Wilcoxon matched pairs test.

Time series from FRAP experiments were drift corrected in Fiji (Schindelin et al., 2012) using the StackReg plugin, and for each experiment, three different z axis profiles were plotted: (1) from the photo-bleached area; (2) from an equivalent area of a neighboring non-photo-bleached AJ; and (3) from an equivalent area of background. The obtained data were normalized using easyFRAP (Rapsomaniki et al., 2012). E-cadherin::GFP (using ubi-cadherin::GFP) data were fitted to a one-phase association curve in GraphPad Prism. Mobile fractions (y value at infinite times) were determined with Prism based on the fitting curves obtained. The p values were calculated with an unpaired two-tailed Student's t test with Welch's correction. For all data, graphical representation and statistical analysis were performed in GraphPad Prism version 6.0 for Mac (GraphPad Software; http://www.graphpad.com). Columns represent mean, and error bars are the SEM of each dataset.

SUPPLEMENTAL INFORMATION

Supplemental Information includes Supplemental Experimental Procedures and five figures and can be found with this article online at http://dx.doi.org/10.1016/j.celrep.2016.03.014.

AUTHOR CONTRIBUTIONS

R.F.W., F.N.A., E.V., and J.J.B. conducted the experiments; F.P. and R.F.W. designed the experiments; and F.P. wrote the paper with the help of R.F.W.

ACKNOWLEDGMENTS

The authors are very grateful to Alan Hall and Dan Jin for sharing their work on Pak4 phosphorylation of hPar6b prior to publication. We also would like to thank Thomas Raabe, Daniel St Johnston, Andreas Wodarz, The Developmental Studies Hybridoma Bank, and Flybase for reagents. This work was funded by an MRC grant (award number 158745) to F.P. E.V. is the recipient of an MRC CDF.

Received: October 1, 2015
Revised: January 19, 2016
Accepted: February 26, 2016
Published: March 24, 2016

REFERENCES

Afonso, C., and Henrique, D. (2006). PAR3 acts as a molecular organizer to define the apical domain of chick neuroepithelial cells. J. Cell Sci. *119*, 4293–4304.

Benton, R., and St Johnston, D. (2003a). A conserved oligomerization domain in Drosophila Bazooka/PAR-3 is important for apical localization and epithelial polarity. Curr. Biol. *13*, 1330–1334.

Benton, R., and St Johnston, D. (2003b). Drosophila PAR-1 and 14-3-3 inhibit Bazooka/PAR-3 to establish complementary cortical domains in polarized cells. Cell *115*, 691–704.

Berger, S., Bulgakova, N.A., Grawe, F., Johnson, K., and Knust, E. (2007). Unraveling the genetic complexity of Drosophila stardust during photoreceptor morphogenesis and prevention of light-induced degeneration. Genetics *176*, 2189–2200.

Bravo-Cordero, J.J., Magalhaes, M.A., Eddy, R.J., Hodgson, L., and Condeelis, J. (2013). Functions of cofilin in cell locomotion and invasion. Nat. Rev. Mol. Cell Biol. *14*, 405–415.

Dan, C., Kelly, A., Bernard, O., and Minden, A. (2001). Cytoskeletal changes regulated by the PAK4 serine/threonine kinase are mediated by LIM kinase 1 and cofilin. J. Biol. Chem. *276*, 32115–32121.

Doerflinger, H., Vogt, N., Torres, I.L., Mirouse, V., Koch, I., Nüsslein-Volhard, C., and St Johnston, D. (2010). Bazooka is required for polarisation of the Drosophila anterior-posterior axis. Development *137*, 1765–1773.

Engl, W., Arasi, B., Yap, L.L., Thiery, J.P., and Viasnoff, V. (2014). Actin dynamics modulate mechanosensitive immobilization of E-cadherin at adherens junctions. Nat. Cell Biol. *16*, 587–594.

Ha, B.H., Morse, E.M., Turk, B.E., and Boggon, T.J. (2015). Signaling, Regulation, and Specificity of the Type II p21-activated Kinases. J. Biol. Chem. *290*, 12975–12983.

Harris, T.J., and Peifer, M. (2004). Adherens junction-dependent and -independent steps in the establishment of epithelial cell polarity in Drosophila. J. Cell Biol. *167*, 135–147.

Hutterer, A., Betschinger, J., Petronczki, M., and Knoblich, J.A. (2004). Sequential roles of Cdc42, Par-6, aPKC, and Lgl in the establishment of epithelial polarity during Drosophila embryogenesis. Dev. Cell *6*, 845–854.

Jin, D., Durgan, J., and Hall, A. (2015). Functional cross-talk between Cdc42 and two downstream targets, Par6B and PAK4. Biochem. J. *467*, 293–302.

Krahn, M.P., Bückers, J., Kastrup, L., and Wodarz, A. (2010). Formation of a Bazooka-Stardust complex is essential for plasma membrane polarity in epithelia. J. Cell Biol. *190*, 751–760.

McDonald, J.A., Khodyakova, A., Aranjuez, G., Dudley, C., and Montell, D.J. (2008). PAR-1 kinase regulates epithelial detachment and directional protrusion of migrating border cells. Curr. Biol. *18*, 1659–1667.

McKinley, R.F., and Harris, T.J. (2012). Displacement of basolateral Bazooka/PAR-3 by regulated transport and dispersion during epithelial polarization in Drosophila. Mol. Biol. Cell *23*, 4465–4471.

Menzel, N., Schneeberger, D., and Raabe, T. (2007). The Drosophila p21 activated kinase Mbt regulates the actin cytoskeleton and adherens junctions to control photoreceptor cell morphogenesis. Mech. Dev. *124*, 78–90.

Menzel, N., Melzer, J., Waschke, J., Lenz, C., Wecklein, H., Lochnit, G., Drenckhahn, D., and Raabe, T. (2008). The Drosophila p21-activated kinase Mbt modulates DE-cadherin-mediated cell adhesion by phosphorylation of Armadillo. Biochem. J. *416*, 231–241.

Morais-de-Sá, E., Mirouse, V., and St Johnston, D. (2010). aPKC phosphorylation of Bazooka defines the apical/lateral border in Drosophila epithelial cells. Cell *141*, 509–523.

Nam, S.C., Mukhopadhyay, B., and Choi, K.W. (2007). Antagonistic functions of Par-1 kinase and protein phosphatase 2A are required for localization of Bazooka and photoreceptor morphogenesis in Drosophila. Dev. Biol. *306*, 624–635.

Rapsomaniki, M.A., Kotsantis, P., Symeonidou, I.E., Giakoumakis, N.N., Taraviras, S., and Lygerou, Z. (2012). easyFRAP: an interactive, easy-to-use tool for qualitative and quantitative analysis of FRAP data. Bioinformatics *28*, 1800–1801.

Schindelin, J., Arganda-Carreras, I., Frise, E., Kaynig, V., Longair, M., Pietzsch, T., Preibisch, S., Rueden, C., Saalfeld, S., Schmid, B., et al. (2012). Fiji: an open-source platform for biological-image analysis. Nat. Methods *9*, 676–682.

Schneeberger, D., and Raabe, T. (2003). Mbt, a Drosophila PAK protein, combines with Cdc42 to regulate photoreceptor cell morphogenesis. Development *130*, 427–437.

Selamat, W., Tay, P.L., Baskaran, Y., and Manser, E. (2015). The Cdc42 Effector Kinase PAK4 Localizes to Cell-Cell Junctions and Contributes to Establishing Cell Polarity. PLoS ONE *10*, e0129634.

Shahab, J., Tiwari, M.D., Honemann-Capito, M., Krahn, M.P., and Wodarz, A. (2015). Bazooka/PAR3 is dispensable for polarity in Drosophila follicular epithelial cells. Biol. Open *4*, 528–541.

St Johnston, D., and Ahringer, J. (2010). Cell polarity in eggs and epithelia: parallels and diversity. Cell *141*, 757–774.

Tian, Y., Lei, L., and Minden, A. (2011). A key role for Pak4 in proliferation and differentiation of neural progenitor cells. Dev. Biol. *353*, 206–216.

Totong, R., Achilleos, A., and Nance, J. (2007). PAR-6 is required for junction formation but not apicobasal polarization in C. elegans embryonic epithelial cells. Development *134*, 1259–1268.

Wallace, S.W., Durgan, J., Jin, D., and Hall, A. (2010). Cdc42 regulates apical junction formation in human bronchial epithelial cells through PAK4 and Par6B. Mol. Biol. Cell *21*, 2996–3006.

Walther, R.F., and Pichaud, F. (2006). Immunofluorescent staining and imaging of the pupal and adult Drosophila visual system. Nat. Protoc. *1*, 2635–2642.

Walther, R.F., and Pichaud, F. (2010). Crumbs/DaPKC-dependent apical exclusion of Bazooka promotes photoreceptor polarity remodeling. Curr. Biol. *20*, 1065–1074.

Wei, S.Y., Escudero, L.M., Yu, F., Chang, L.H., Chen, L.Y., Ho, Y.H., Lin, C.M., Chou, C.S., Chia, W., Modolell, J., and Hsu, J.C. (2005). Echinoid is a component of adherens junctions that cooperates with DE-Cadherin to mediate cell adhesion. Dev. Cell *8*, 493–504.

Zihni, C., Munro, P.M., Elbediwy, A., Keep, N.H., Terry, S.J., Harris, J., Balda, M.S., and Matter, K. (2014). Dbl3 drives Cdc42 signaling at the apical margin to regulate junction position and apical differentiation. J. Cell Biol. *204*, 111–127.

Cell Reports, Volume *15*

Supplemental Information

Pak4 Is Required during Epithelial Polarity Remodeling through Regulating AJ Stability and Bazooka Retention at the ZA

Rhian F. Walther, Francisca Nunes de Almeida, Evi Vlassaks, Jemima J. Burden, and Franck Pichaud

Supplementary Figure 1: Apico-basal polarity remodeling in the developing photoreceptor

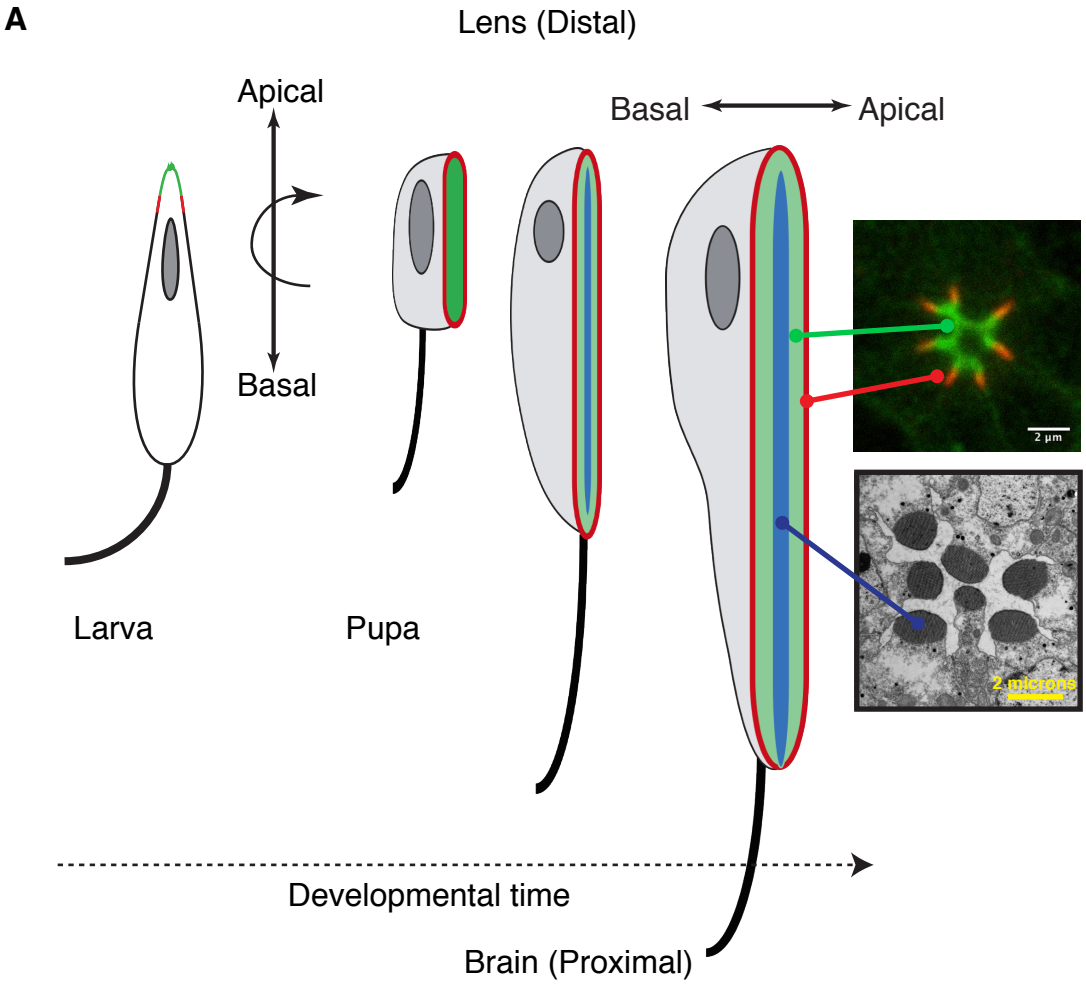

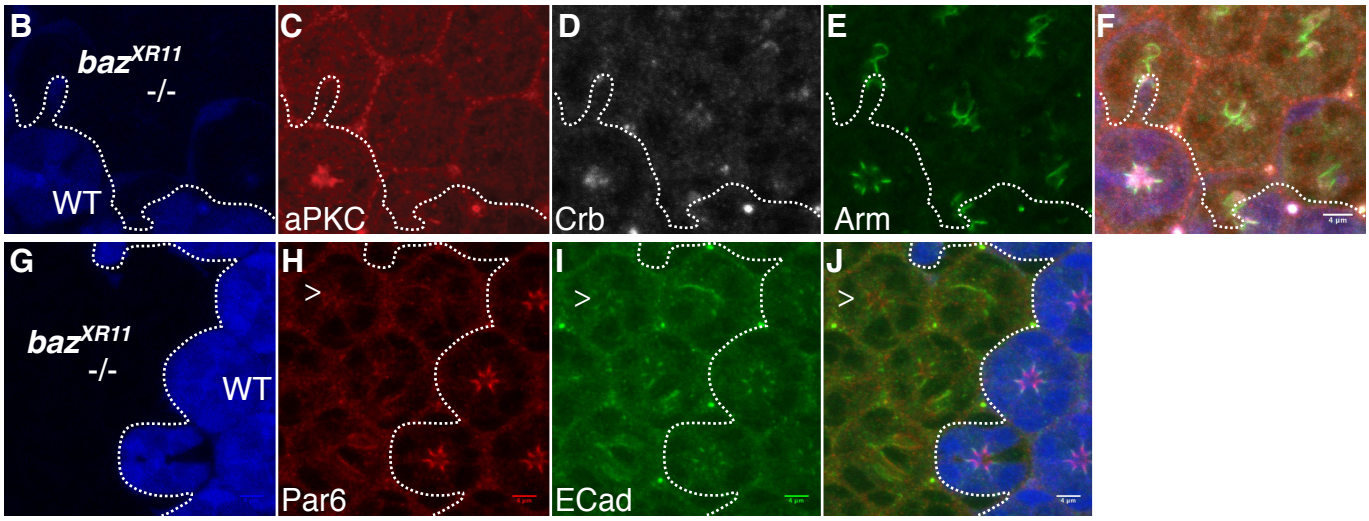

Supplementary Figure 2: *mbt* regulates apical membrane differentiation

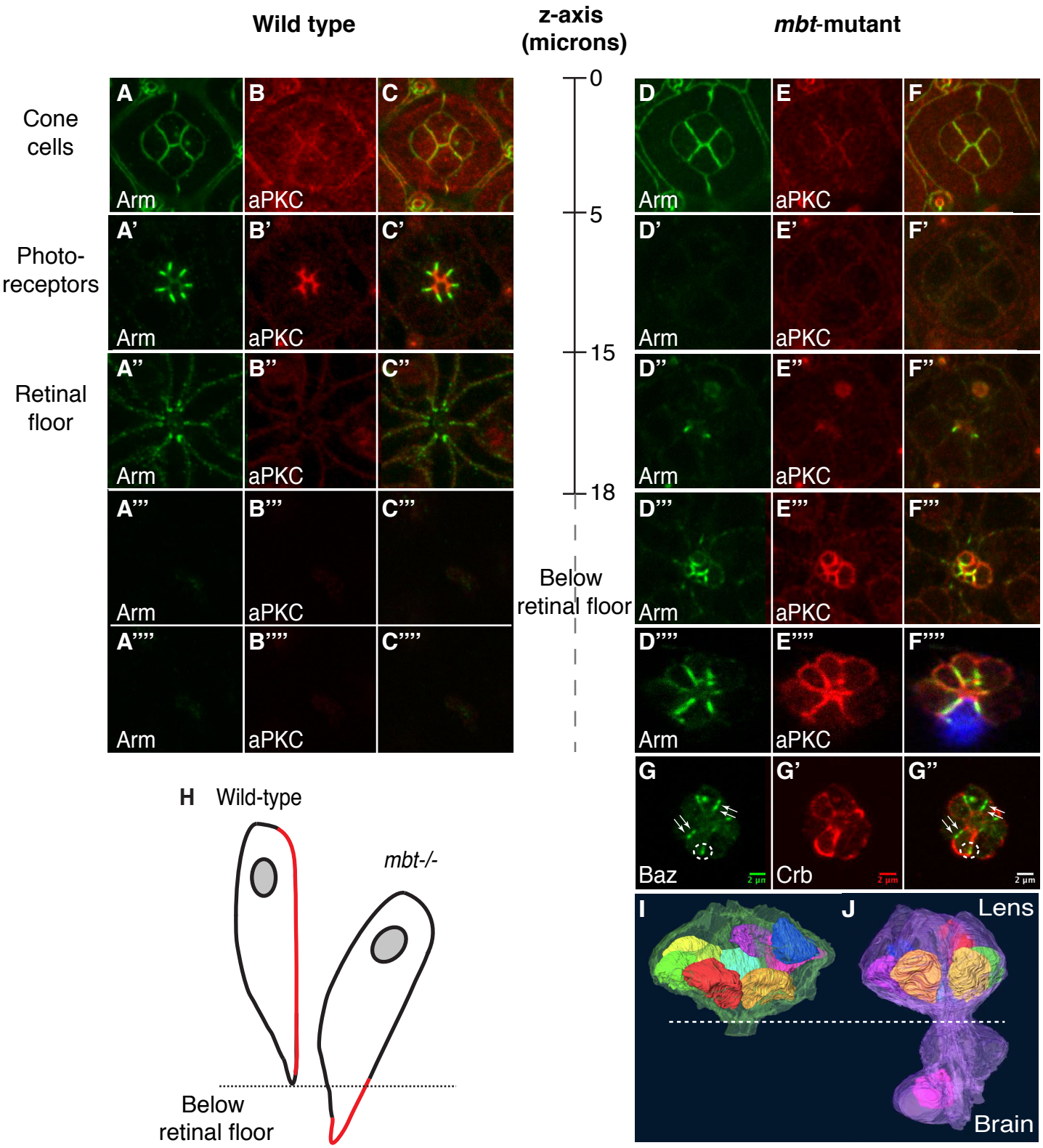

Supplementary Figure 3: Regulated Mbt kinase activity is required during apical membrane differentiation

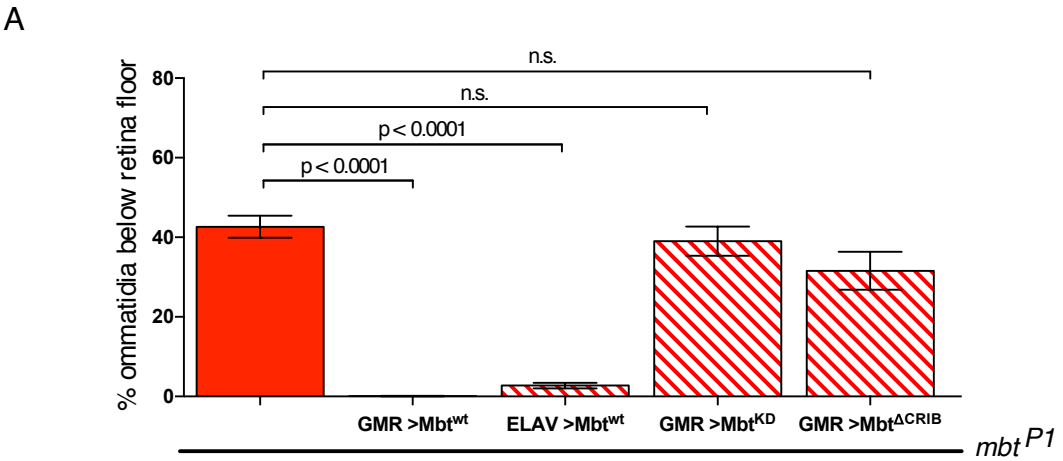

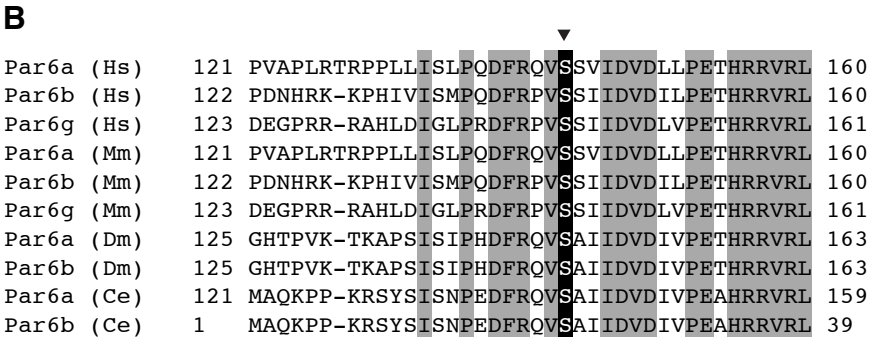

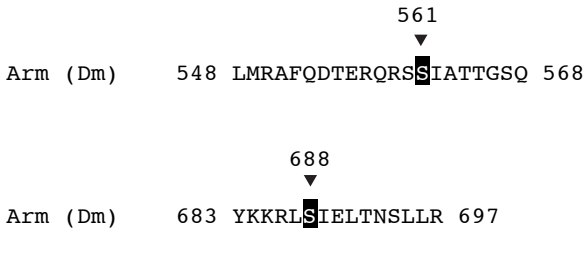

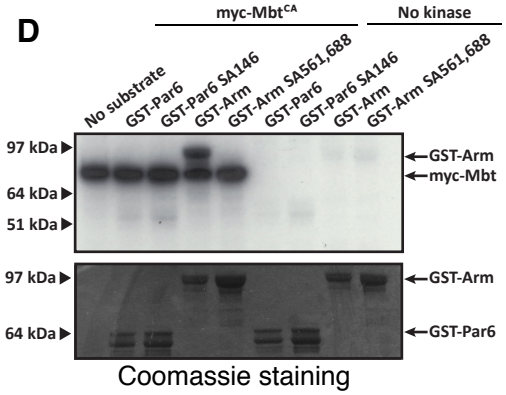

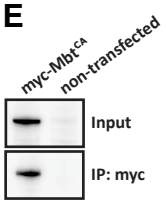

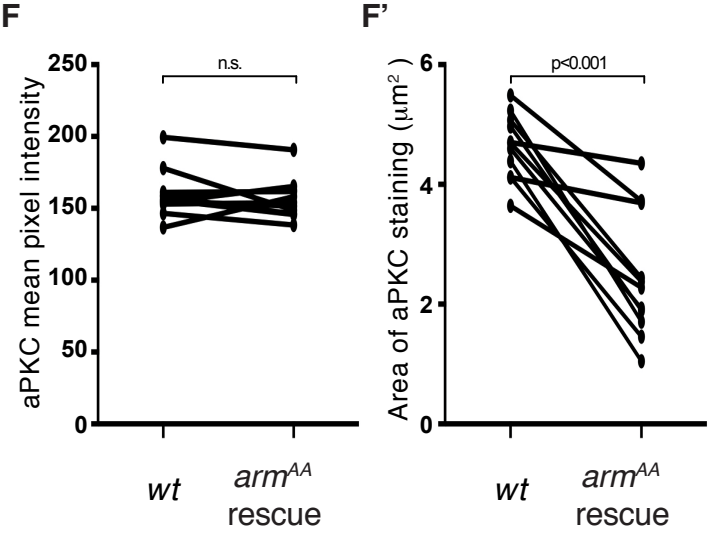

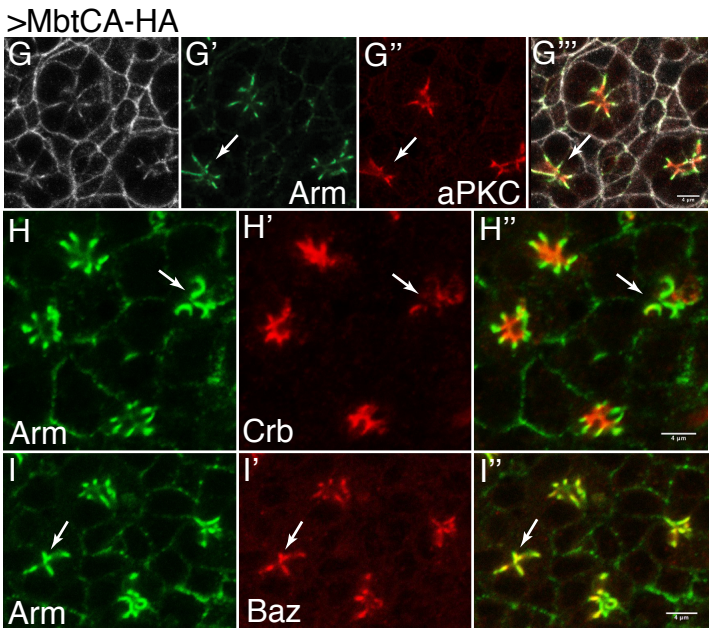

Supplementary Figure 4: Arm phosphorylation regulates *AJ* material stability

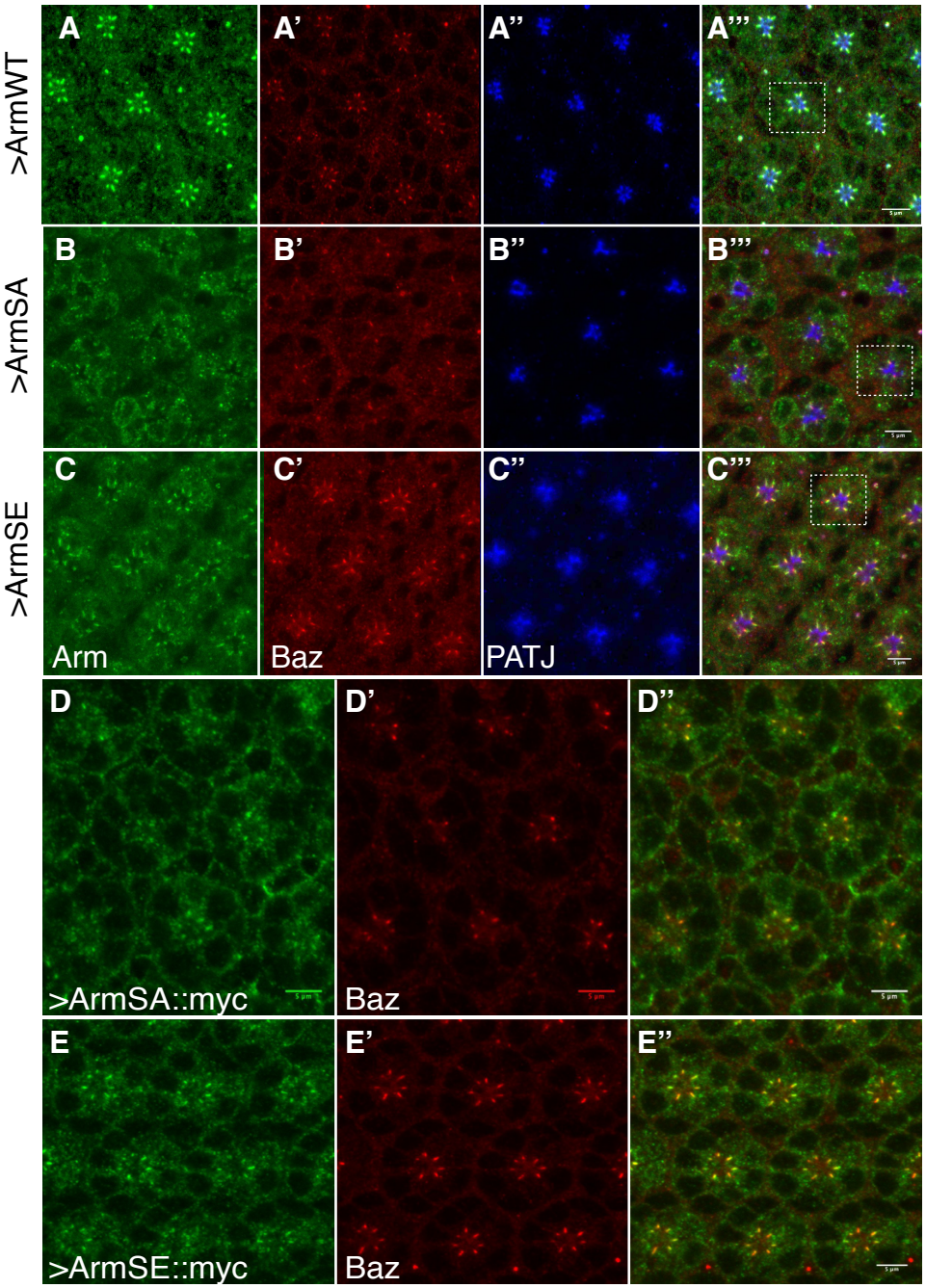

Supplementary Figure 5: Par1 localization and function during photoreceptor morphogenesis

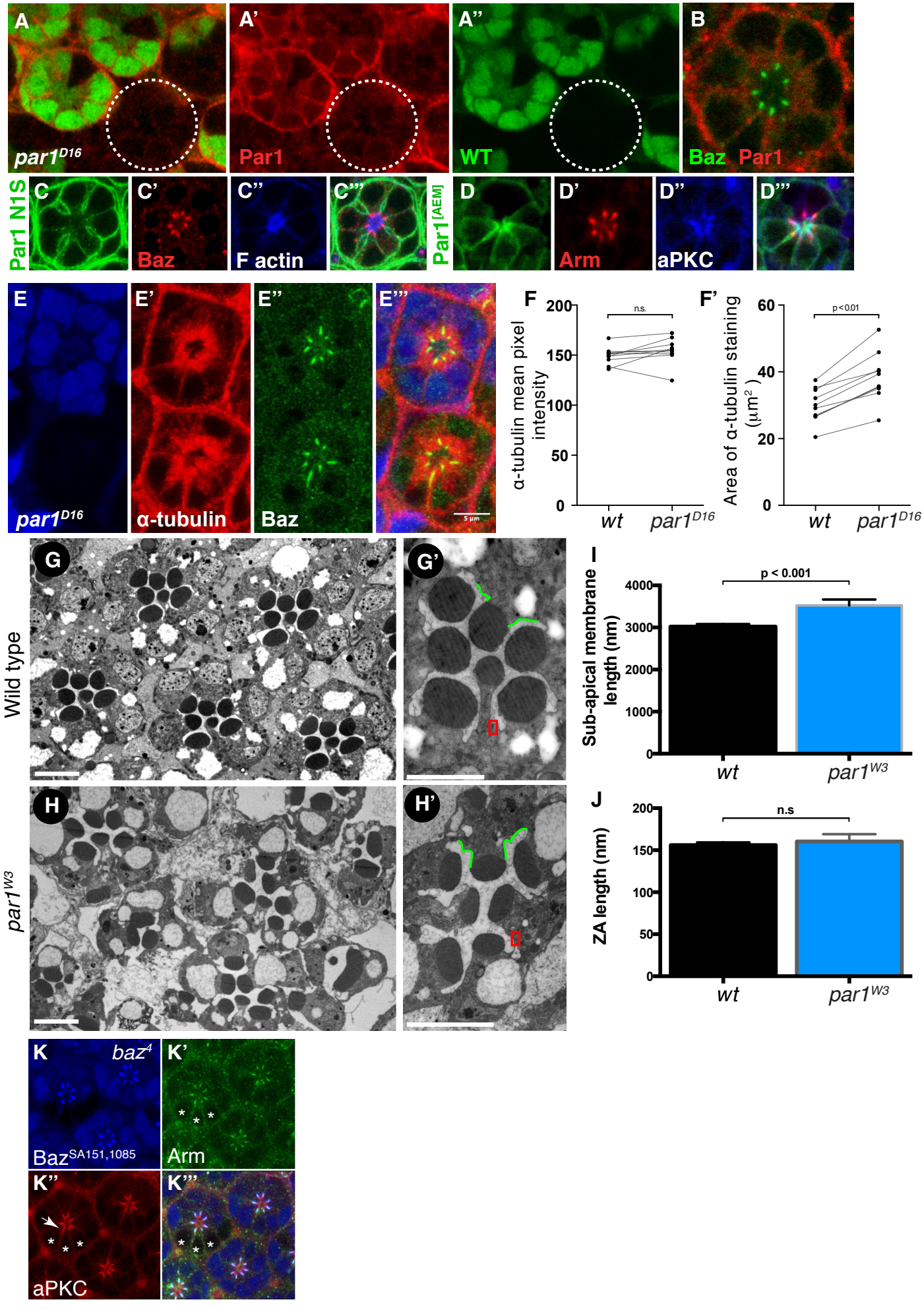

Supplementary Figure 1: Apico-basal polarity remodeling in the developing photoreceptor (A) During pupation, the apico-basal axis of the photoreceptor rotates 90 degrees as the cell undergoes morphogenesis. During pupal development, the new apical membrane domains are subsequently formed over time. *ZA* (red), sub-apical membrane (green) and stack of microvilli (blue). A representative confocal section of a wild type pupal ommatidium and electron micrograph of an adult ommatidum are shown, indicating the respective apical membrane domains. (B-F) baz^{XR11} mutant clone in the pupal retina. Mutant cells lack GFP (blue). aPKC (red), Crb (gray) and Arm (green). (G-J) baz^{XR11} mutant clone in the pupal retina. Par6 (red), E-cadherin (green). A white arrowhead points to residual Par6 staining (H) and *AJ* domains (I). Scale bars = 4 microns.

Supplementary Figure 2: *mbt* regulates apical membrane differentiation (A-F) Series of confocal sections along the lens to brain axis of a wild type ommatidium (A-C) and an mbt^{P1} mutant (D-F). Arm (green), aPKC (red) and merged images are shown in (C-C'''' and F– F''''). (A-F) Cone cell *AJ*. (A'-F') Confocal sections taken at the level of the photoreceptors. (A''-F'') Confocal sections of the retinal floor. In (D'''- F''' and D''''- F'''') consecutive sections below the retina are labeled BRF (Below Retinal Floor). (G-G'') Confocal section of an ommatidium mutant for mbt^{P1} stained for Baz (green) and Crb (red) imaged below the retinal floor. White arrows indicate tandem accumulations of *AJ* material while basally shifted *AJ* material is highlighted by a dashed circle. A merged image is shown in (G''). Scale bars = 2 microns.

(H) Representation of a wild type (left) and *mbt*^{P1} mutant ommatidium (right). The floor of the retina is represented as a dashed line. The apical membrane (i.e sub-apical membrane and *ZA*) is represented as a red line. (I-J) 3D rendering of serial electron microscopy (3View) performed on a wild type (I) and *mbt*^{P1} mutant (J) developing ommatidium at 45% after puparium formation. Photoreceptor nuclei are in solid colors. Cell membranes are in green (wild type) and purple (*mbt*^{P1}). The floor of the retina is highlighted by a dashed white line.

Supplementary Figure 3: Regulated Mbt kinase activity is required during apical membrane differentiation (A) Delamination phenotype in *mbt*^{P1} retina and *mbt*^{P1} expressing the wild type, kinase dead (KD) or ΔCRIB form of Mbt. For each genotype a minimum of 4 retinas were quantified. Columns represent mean and error bars are the SEM of each data set. Statistical significance was determined with one-way ANOVA and Dunnett's multiple comparison test for parametric samples. (B) Alignment of Par6 (Jin et al., 2015). (C) Serine residues 561 and 688 in Arm (Menzel et al., 2008). (D) *In vitro* phosphorylation assay. (E) Myc::Mbt^{CA} was expressed and isolated from S2 cells. (F) Mean pixel intensity of aPKC (F) and aPKC area (F') in paired wild type and *arm*^{3} mutant ommatidia expressing ArmSA561,688::myc. Statistical significance was determined using the Wilcoxon matched pairs test. (G-I) Overexpression of MbtCA (gray). (G') Arm (green) and (G'') aPKC (red). White arrows in G' and G'' indicate an apical domain where no separation of Arm from aPKC occurs. (H) Arm (green) and

(H') Crb (red). (I) Arm (green) and (I') Baz (red). (H-H') A white arrow highlights a poorly differentiated apical domain. (I-I'') A white arrow highlights an ommatidium with defects in apical-basal polarity. Scale bars: 4 microns.

Supplementary Figure 4: Arm phosphorylation regulates *AJ* material stability (A) Overexpression of Arm::myc. In (A-C), Arm (green), Baz (red), PATJ (blue). (B) Overexpression of ArmSA561,688::myc and (C) ArmSE561,688::myc. (D) Overexpression of ArmSA561,688::myc and (E) ArmSE561,688::myc. Myc (green), Baz (red). Scale bars 5 microns.

Supplementary Figure 5: Par1 localization and function during photoreceptor morphogenesis (A-A'') $par1^{D16}$ mutant cells lack nuclear GFP (green). Par1 (red). (B) Par1 (red) and Baz (green). (C-C''') Par-N1S::GFP transgene (green), Baz (red) and F-Actin (blue). (D-D''') Par1-N1S::GFP (AEM) (green), Arm (red) and aPKC (blue). (E-E''') Photoreceptors mutant for $par1^{D16}$ lack nuclear GFP (blue). α-tubulin (red), Baz (green). (F-F') Mean pixel intensity of α-tubulin immunofluorescence (F) and total area of α-tubulin fluorescence (F') in paired wild type and $par1^{D16}$ mutant ommatidia. In (F) and (F'), statistical significance was determined using the Wilcoxon matched pairs test. (G-H) Electron microscopy of a wild type retina (G-G') and a $par1^{W3}$ mutant retina (H-H'). A *ZA* is boxed in red and a sub-apical membrane is highlighted in green in (G') and (H'). Scale bars = 2 microns. (I-J) Length of the sub-apical membrane (I) and *ZA* (J) in wild type and $par1^{W3}$ retina. Columns represent mean and error bars are the SEM of each data set.

(K) *baz*^{4} mutant cells lacking GFP (blue) are highlighted by a white star. The blue channel is also used to show the BazSA151,1085::GFP protein. Arm (green), aPKC (red). A white arrow points to the rescue of aPKC localization.

Fly strains and genetics

The following genotypes were used:

Both the null allele *mbt^{P1} and* hypomorphic allele *mbt^{P3}* (Schneeberger and Raabe, 2003) were used all through this study.

mbt^{P1}FRT19A/FRT19AUbiGFP;eyflp (this work), (Newsome et al., 2000).

w,baz^{4}FRT9.2/ FRT9.2 UbiGFP;*eyflp*. (Nusslein-Volhard et al., 1987).

w,baz^{XR11}FRT19A/ FRT19A UbiGFP;*eyflp* and *w,baz^{EH747}FRT19A/ FRT19A UbiGFP*;*eyflp* (Shahab et al., 2015).

w,baz^{4},sdt^{XP96} FRT9.2/ FRT9.2 UbiGFP;*eyflp* (Muller and Wieschaus, 1996).

mbt^{P1}, baz^{4} FRT9.2/FRT9.2 UbiGFP;eyflp (this work).

w,hsflp;;crb^{11A22}FRT82B/ FRT82B UbiGFP (Tepass et al., 1990); *w, eyflp ; aPKC^{k06403} FRT42D/ FRT42D UbiGFP* (Wodarz et al., 2000). *w,arm^{3} FRT101/FRT101 UbiGFP;eyflp* (Peifer et al., 1991). *w; EGUF, par1^{w3} FRT42D/FRT42D GMR-hid,cl* (Shulman et al., 2000).

eyFLP/+;par1$^{\Delta 16}$FRTG13/FRTG13 UbiGFP. GMR-Gal4/UAS-par1N1S::GFP; GMR-Gal4/UAS-par1::N1S GFP (AEM); (Doerflinger et al., 2007); *GMR-Gal4/UAS-baz::GFP; and bazSA151,1085::GFP* (Benton and St Johnston, 2003). *;GMR-Gal4/ UAS-bazSA151,1085::GFP; mbt^{P1}/Y*; *GMR-Gal4/UAS-baz::GFP;. mbt^{P1}/Y; GMR-Gal4/UAS-bazSA151,1085::GFP;. UAS-mbt^{CA}/CyO; GMR-Gal4/TM2*. (Menzel et al., 2007). *mbt^{P1}/Y; GMR-Gal4/+;UAS-mbt^{WT}/+. mbt^{P1}/Y; ELAV-Gal4/+;UAS-mbt^{WT}/+. mbt^{P1}/Y; GMR-Gal4/UAS-mbt^{CA};. mbt^{P1}/Y*; *GMR-Gal4/+;UAS-mbt$^{\Delta CRIB}$/+* (Menzel et al., 2007). *GMR-Gal4/+; UASt-arm::myc/+* (this work). *GMR-Gal4/+; UASt-armSA561,688::myc/+* (this work). *GMR-Gal4/+ ; UASt-armSE561,688::myc/+* (this work). *w,arm^{3} FRT101/FRT101*

UbiGFP;eyflp/GMR-Gal4; UASt-arm::myc/+;. w,arm^{3} FRT101/FRT101 UbiGFP;eyflp/GMR-Gal4; UASt-armSA561,688::myc/+;. *w,arm^{3} FRT101/FRT101 UbiGFP;eyflp/GMR-Gal4*; *UASt-armSE561,688::myc/+*;. General fly cultures and crosses were carried out at 25^{o}C.

Transgenic flies

Clone LD23131 encoding Armadillo cDNA was obtained from the Drosophila Genomics Resource Center and then subcloned into the pENTR™/D-TOPO® vector (Invitrogen). Residues S561 and S688 were mutated to alanine or glutamic acid using the QuikChange Lightning Multi Site-Directed Mutagenesis Kit. Following sequence verification (MWG Eurofins), the wild-type, SA561,688 and SE561,688 entry clones were used for Gateway cloning (Invitrogen) into the pTWM destination vector (Murphy lab) for expression of a C-terminally Myc tagged protein under the control of the UAST promoter. Injections were performed by BestGene (Chino Hills, CA).

Kinase Assay

GST-tagged Par6, Par6SA146, Arm and ArmSA561,688 were cloned into a pDEST15 vector containing an N-terminal GST tag using the Gateway Cloning System (Invitrogen). Bacteria were lysed by sonication in Lysis Buffer (50 mM Tris HCl pH7.6, 50 mM NaCl, 5 mM $MgCl_2$, 0.5% Triton X-100, 10 mM DTT) in the presence of protease inhibitor (EDTA-free Complete Protease Inhibitor [Roche]). GST fusion proteins were purified using Glutathione Sepharose 4 Fast Flow beads (GE Healthcare) and then washed (50 mM Tris HCl pH 7.4, 50 mM NaF, 300 mM NaCl, 1 % Triton X-100, 1 mM DTT, EDTA-

free Complete Protease inhibitor), eluted (40 mM Glutathione, 50 mM Tris HCl, pH 8.0), and dialyzed against lysis buffer with 40 % glycerol.

Drosophila Schneider S2 cells (DGRC) were transiently transfected with pActin-Myc::Mbt^{CA} (S492N, S521E) and lysed in 50 mM Tris HCl pH 7.5, 150 mM NaCl, 1 % Triton X-100, 5 mM DTT, EDTA). The lysates were incubated with 4 µg of anti-myc agarose beads (Sigma) for 1h at 4°C. The beads were washed with the kinase buffer (20 mM HEPES, pH 7.6, 150 mM NaCl, 20 mM $MgCl_2$, 10 µL/mL phosphatase inhibitor [Sigma], 20 µM ATP). Beads with kinase were split in 20 µL fractions and then mixed with 30 µg of each substrate GST fusion protein as well as 1 µL of [ɣ-^{32}P]-ATP (5 µCi). Each condition was incubated at 30^{o}C for 30 min. The proteins were separated by SDS-PAGE and visualized by autoradiography.

Electron microscopy

Electron microscopy was performed as in (Pinal et al., 2006) using a Tecnai G2 Spirit transmission electron microscope (FEI, The Netherlands) equipped with a Morada CCD camera (Olympus Soft Imaging Systems). Image quantification was performed using iTEM software.

For serial block face scanning electron microscopy, samples were prepared using a combinatorial heavy metal staining protocol involving thiocarbohydrazide, double osmication and *en bloc* Walton's lead aspartate as described by Ellisman and colleagues; http://ncmir.ucsd.edu/sbfsem-

protocol.pdf. Embedded samples were oriented, re-embedded, and regions of interest were identified from 70nm sections examined by TEM. The region of interest was then excised and mounted with cyanoacrylate glue onto specimen pins. These samples were further trimmed before being coated with gold palladium and mounted in the 3View microtome (Gatan, USA). Once aligned, the sample and microtome were returned to the SEM chamber and put under vacuum. The regions of interest on the block face were re-located in the SEM using backscattered electron detection and the imaging and cutting parameters were optimised for each sample. Data sets of 999 sections were collected with section thickness 75-100nm in a Zeiss Sigma FEG-SEM coupled to the Gatan 3View. Data was imported into Amira (VSG, France), where the cells of interest were manually segmented, reconstructed and rendered in 3D.

References

Benton, R., and St Johnston, D. (2003). Drosophila PAR-1 and 14-3-3 inhibit Bazooka/PAR-3 to establish complementary cortical domains in polarized cells. Cell *115*, 691-704.

Menzel, N., Schneeberger, D., and Raabe, T. (2007). The Drosophila p21 activated kinase Mbt regulates the actin cytoskeleton and adherens junctions to control photoreceptor cell morphogenesis. Mech Dev *124*, 78-90.

Muller, H.A., and Wieschaus, E. (1996). armadillo, bazooka, and stardust are critical for early stages in formation of the zonula adherens and maintenance of the polarized blastoderm epithelium in Drosophila. J Cell Biol *134*, 149-163.

Newsome, T.P., Asling, B., and Dickson, B.J. (2000). Analysis of Drosophila photoreceptor axon guidance in eye-specific mosaics. Development *127*, 851-860.

Nusslein-Volhard, C., Frohnhofer, H.G., and Lehmann, R. (1987). Determination of anteroposterior polarity in Drosophila. Science *238*, 1675-1681.

Peifer, M., Rauskolb, C., Williams, M., Riggleman, B., and Wieschaus, E. (1991). The segment polarity gene armadillo interacts with the wingless signaling pathway in both embryonic and adult pattern formation. Development *111*, 1029-1043.

Pinal, N., Goberdhan, D.C., Collinson, L., Fujita, Y., Cox, I.M., Wilson, C., and Pichaud, F. (2006). Regulated and polarized PtdIns(3,4,5)P3 accumulation is essential for apical membrane morphogenesis in photoreceptor epithelial cells. Current biology : CB *16*, 140-149.

Schneeberger, D., and Raabe, T. (2003). Mbt, a Drosophila PAK protein, combines with Cdc42 to regulate photoreceptor cell morphogenesis. Development *130*, 427-437.
Shahab, J., Tiwari, M.D., Honemann-Capito, M., Krahn, M.P., and Wodarz, A. (2015). Bazooka/PAR3 is dispensable for polarity in Drosophila follicular epithelial cells. Biology open *4*, 528-541.
Shulman, J.M., Benton, R., and St Johnston, D. (2000). The Drosophila homolog of C. elegans PAR-1 organizes the oocyte cytoskeleton and directs oskar mRNA localization to the posterior pole. Cell *101*, 377-388.
Tepass, U., Theres, C., and Knust, E. (1990). crumbs encodes an EGF-like protein expressed on apical membranes of Drosophila epithelial cells and required for organization of epithelia. Cell *61*, 787-799.
Wodarz, A., Ramrath, A., Grimm, A., and Knust, E. (2000). Drosophila atypical protein kinase C associates with Bazooka and controls polarity of epithelia and neuroblasts. J Cell Biol *150*, 1361-1374.